Harmonic Green's functions for flexural waves in semi-infinite plates with arbitrary boundary conditions and high-frequency approximation for convex polygonal plates

Jacques Cuenca*, François Gautier, Laurent Simon

LAUM, CNRS, Université du Maine, Avenue Olivier Messiaen, 72085 Le Mans, France

ARTICLE INFO

ABSTRACT

This paper provides a method for obtaining the harmonic Green's function for flexural waves in semi-infinite plates with arbitrary boundary conditions and a high frequency approximation of the Green's function in the case of convex polygonal plates, by using a generalised image source method. The classical image source method consists in describing the response of a point-driven polygonal plate as a superposition of contributions from the original source and virtual sources located outside of the plate, which represent successive reflections on the boundaries. The proposed approach extends the image source method to plates including boundaries that induce coupling between propagating and evanescent components of the field and on which reflection depends on the angle of incidence. This is achieved by writing the original source as a Fourier transform representing a continuous sum of propagating and evanescent plane waves incident on the boundaries. Thus, the image source contributions arise as continuous sums of reflected plane waves. For semi-infinite plates, the exact Green's function is obtained for an arbitrary set of boundary conditions. For polygonal plates, a high-frequency approximation of the Green's function is obtained by neglecting evanescent waves for the second and subsequent reflections on the edges. The method is compared to exact and finite element solutions and evaluated in terms of its frequency range of applicability.

1. Introduction

Flexural vibrations of thin plate structures used in automotive, aeronautic and aerospace engineering applications are highly responsible for radiated noise and structural damage, for which accurate predictive tools are crucial. In particular, mid- and high-frequency vibrations of plates require the development of new methods and models due to the increasing demand in terms of comfort and reliability of structures.

The knowledge of the harmonic Green's function for flexural waves in a polygonal plate having arbitrary shape and arbitrary boundary conditions is of valuable interest, for it can be considered as the most elementary and general problem in many applications. Such has been the aim of a vast number of papers and monographs for various decades. The most popular methods are based on modal expansion (see e.g. Refs. [1–7] and the references therein). However, analytical modal expansion is limited to few geometries and sets of boundary conditions. Furthermore, modal expansion in general

* Corresponding author. Tel.: +44 23 8059 5930; fax: +33 243833520.
E-mail addresses: jacques.cuenca.etu@univ-lemans.fr, j.cuenca@soton.ac.uk (J. Cuenca), francois.gautier@univ-lemans.fr (F. Gautier), laurent.simon@univ-lemans.fr (L. Simon).

becomes impractical in the presence of high damping and at high frequencies, where modal density is significant, so that considering modes individually is not appropriate. An implicit representation of Green's function of a polygonal plate of arbitrary shape and having arbitrary boundary conditions can be obtained by using the integral formulation [8]. The numerical implementation of the integral formulation is performed by using the boundary element method (BEM) [9,10], which relies on the discretisation of the boundary and is well-adapted to arbitrarily shaped enclosed domains. However, the maximum discretisation interval must be significantly smaller than the wavelength, which is restrictive in terms of computational efficiency at high frequencies.

Nowadays, the most commonly used numerical tools for predicting the vibrations of thin structures are finite element methods (FEMs) (see e.g. Ref. [11]) and statistical energy analysis (SEA) [12]. Similar to BEM, FEM is known to provide solutions that converge towards the exact solutions as the size of the elements tends to zero. However, its computational limitations with frequency are comparable to those of BEM. On the other hand, SEA is applicable above a lower frequency limit and does not present a higher frequency limit [13]. However, the main restrictions of classical SEA are that it provides spatially averaged power for each substructure of the considered system and that narrow-band or harmonic excitation are difficult to deal with [14]. Both FEM and SEA are well known and accepted by researchers and engineers and they are complementary in terms of their frequency range of application. However, due to their intrinsic limitations, other methods have arisen, aiming at extending FEM to higher frequencies or providing SEA with the capability of predicting the spatial distribution of vibrations within a given structure. A complete review of such methods would be out of scope here and hence the reader is referred to Refs. [15–17] and the references therein. An alternative method that has been given significant attention for mid- and high-frequency analysis is the ray-tracing method. The latter allows to estimate the energy distribution inside enclosed spaces and has been used efficiently for flexural motion in thin plates [15]. However, it is based on the assumption that every wave in the domain is uncorrelated from any other, which makes it impossible for it to account for interferences. Furthermore, the ray method considers only propagating waves, for which it is unable to predict the complete flexural wave field in a thin plate [18].

Recently, attention has been paid to the image source method as an alternative predictive tool for high frequency flexural vibrations of polygonal plates. The classical image source method consists in representing successive wave reflections on the boundaries of a point-driven polygonal plate as virtual sources. Such virtual sources are obtained from successive symmetries of the original source with respect to the edges of the plate. Accordingly, the amplitudes of the image sources are given as the product of the amplitude of the original source (i.e. the driving point) and the reflection coefficients of the successive edges at which reflection occurs. Gunda et al. [19] showed that the image source method, as commonly used in room acoustics [20], is efficient for obtaining the response of beams and rectangular plates with simply supported and roller supported plates. In a previous paper [21], the authors examined the case of arbitrarily shaped convex polygonal plates with all edges simply supported, by using the image source method. The method provides exact Green's functions of plates of four polygonal geometries and gives efficient approximations in the case of convex polygonal plates of arbitrary geometry. The main feature of the method is that the accuracy of the computed responses increases with frequency and structural damping, contrarily to modal expansion or finite element methods. Therefore, it can be used as an alternative tool for studying the vibrations of polygonal plates at high frequencies and for highly damped regimes.

The fundamental limitation of the classical image source method is that it is restricted to the case of polygonal plates with boundaries that are characterised by a constant reflection coefficient, which is the case for simply supported and roller supported edges. Reflection on edges with more general boundary conditions, involves wave conversion between propagating and evanescent components of the field and depends on the angle of incidence of waves and on frequency [22]. The most extensive work on such types of boundary conditions has been done by Gunda et al. [23], who derived the exact harmonic Green's function of a semi-infinite plate in the particular cases of clamped and free edges. To the best of our knowledge, the case of arbitrary boundary conditions has not been treated and needs further analysis.

The purpose of this paper is to extend the image source method to arbitrary boundary conditions in order to obtain exact harmonic Green's functions for semi-infinite plates and approximated harmonic Green's functions for convex polygonal plates. The key point of the method consists in describing the source as a continuous sum of plane waves. Using the reflection matrix of each edge, the successive reflections on the boundaries are described by classical reflection laws for plane waves and are interpreted as generalised image sources. The plate response is then obtained as a superposition of the image source contributions.

The paper is organised as follows. First, the Green's function of an infinite plate is expressed as a continuous sum of propagating and evanescent plane waves, which describes the original source. A general expression of the exact harmonic Green's function of a semi-infinite plate is then obtained for an arbitrary set of boundary conditions. For polygonal plates, the semi-infinite plate Green's function is used at each edge for calculating the contributions of image sources, which represent successive reflections of waves on the boundaries. The approximation of the contributions of image sources corresponding to the second and subsequent reflections by neglecting evanescent waves is then discussed. The results are compared to the exact solution on a square plate and to a finite element solution on an arbitrary polygonal plate, both including simply supported and clamped edges.

2. Green's function of an infinite plate

Consider an infinite plate harmonically excited at point $\mathbf{r}_0 = (\xi_0, \mu_0)$, perpendicularly to the (ξ, μ) plane, as shown in Fig. 1. The time factor $e^{-j\omega t}$ is implicit in the following, ω being the excitation circular frequency, and the Sommerfeld
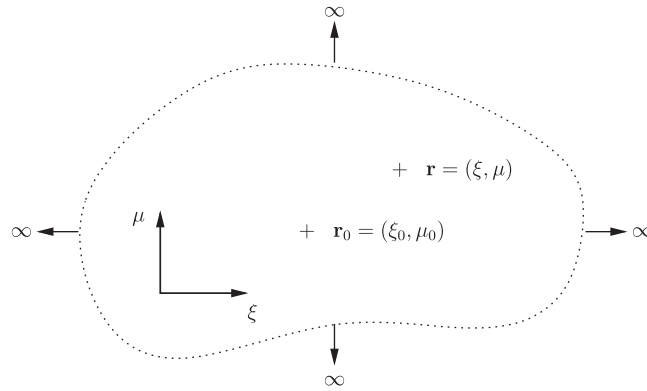
Fig. 1. Green's problem for an infinite plate. $\mathbf{r}_0$, source point; $\mathbf{r}$, observation point.

radiation condition [24] is henceforth assumed. The Green's function of flexural vibrations G_∞ follows the equation [22]

$$D(\nabla^4 - k_f^4)G_\infty(\mathbf{r},\mathbf{r}_0; k_f) = \delta(\mathbf{r}-\mathbf{r}_0), \qquad (1)$$

where the flexural rigidity D depends on Young's modulus E, Poisson's ratio v and the plate thickness h in the form

$$D = \frac{Eh^3}{12(1-v^2)} \qquad (2)$$

and the flexural wavenumber takes the form

$$k_f = \left(\omega^2 \frac{\rho h}{D}\right)^{1/4}, \qquad (3)$$

where ρ is the density of the plate material. According to the time dependence $\mathrm{e}^{-j\omega t}$, structural damping is included in Young's modulus by writing

$$E = E_0(1-j\eta), \qquad (4)$$

where η is the structural damping ratio.

For modelling semi-infinite and polygonal plates, discussed later on in Sections 3 and 4, the Green's function of the infinite plate G_∞ describes the direct contribution of the source to the displacement field of the plate, which is also the incident field on the boundaries. Thus, it is convenient to write G_∞ in rectangular coordinates in order to describe wave reflection in a local coordinate system for each boundary. For such purpose, we use arbitrarily oriented coordinates (ξ,μ), where ξ is referred to as the axial coordinate, collinear to a given boundary, and μ is referred to as the transverse coordinate, normal to the boundary. The Green's function G_∞ is then obtained using one-dimensional Fourier transform of Eq. (1) on coordinate ξ, as detailed in Appendix A, and can be written as

$$G_\infty(\xi,\mu,\xi_0,\mu_0; k_f) = \frac{j}{8\pi k_f^2 D} \int_{-\infty}^{+\infty} \mathrm{e}^{jk_\xi(\xi-\xi_0)} \left(\frac{\mathrm{e}^{j\sqrt{k_f^2-k_\xi^2}|\mu-\mu_0|}}{\sqrt{k_f^2-k_\xi^2}} + j\frac{\mathrm{e}^{-\sqrt{k_f^2+k_\xi^2}|\mu-\mu_0|}}{\sqrt{k_f^2+k_\xi^2}} \right) dk_\xi, \qquad (5)$$

which appears as a sum of plane waves. Fig. 2 shows the transverse wavenumbers $k_\mu^{(1)} = \sqrt{k_f^2-k_\xi^2}$ and $k_\mu^{(2)} = j\sqrt{k_f^2+k_\xi^2}$ as functions of the axial wavenumber k_ξ. As a convention, the principal square root (i.e. the root whose real part is positive) is henceforth used. From Fig. 2 and Eq. (5), it can be observed that the term $\mathrm{e}^{j\sqrt{k_f^2-k_\xi^2}|\mu-\mu_0|}/\sqrt{k_f^2-k_\xi^2}$ represents a propagating wave for $|k_\xi| < |k_f|$ and an evanescent wave for $|k_\xi| > |k_f|$. Similarly, the term $j\mathrm{e}^{-\sqrt{k_f^2+k_\xi^2}|\mu-\mu_0|}/\sqrt{k_f^2+k_\xi^2}$ represents an evanescent wave for all values of k_ξ. Note that the flexural wavenumber k_f is complex because of structural damping, as defined in Eq. (4), and has an imaginary part that is small compared to its real part. This implies that the propagating term presents a slight decrease in amplitude with distance and that the evanescent term presents a slow oscillatory behaviour.
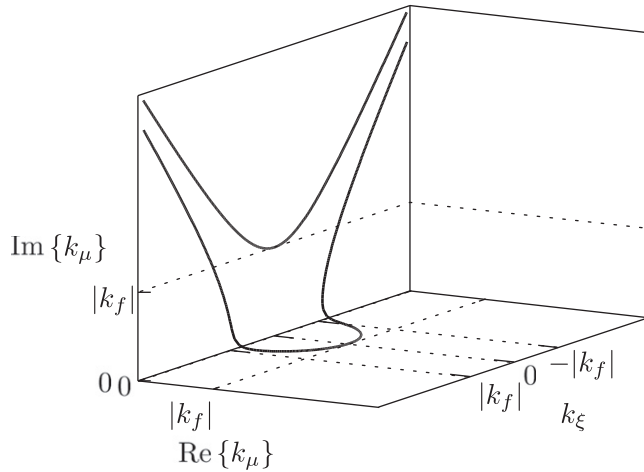
Fig. 2. Transverse wavenumbers as functions of k_ξ. Lower curve, $k_\mu^{(1)} = \sqrt{k_f^2 - k_\xi^2}$; upper curve, $k_\mu^{(2)} = j\sqrt{k_f^2 + k_\xi^2}$.
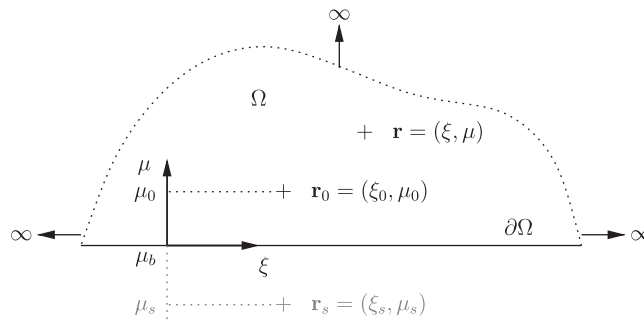
Fig. 3. Green's problem for a semi-infinite plate. $\mathbf{r}_0$, original source; $\mathbf{r}_s$, image source; $\mathbf{r}$, observation point.

3. Green's function of a semi-infinite plate

3.1. Formulation of the problem

Considering a semi-infinite plate Ω, excited by a point source at $\mathbf{r}_0$ as represented in Fig. 3, Green's function G_Ω is the solution of the generic set of equations

$$\begin{cases} D(\nabla^4 - k_f^4))G_\Omega(\mathbf{r}, \mathbf{r}_0; k_f) = \delta(\mathbf{r} - \mathbf{r}_0), & \mathbf{r} \in \Omega, \quad \text{(a)} \\ \text{Boundary conditions,} & \mathbf{r} \in \partial\Omega, \quad \text{(b)} \end{cases} \tag{6}$$

where the boundary conditions are here assumed to be linear and homogeneous along the edge. As in the case of the infinite plate discussed above, the Sommerfeld radiation condition is here considered. The displacement field at $\mathbf{r}$ can be obtained as the superposition of the infinite plate Green's function G_∞ and the reflected field from the boundary, denoted G_s, which is later on interpreted as the contribution of an image source located at point $\mathbf{r}_s$. The general solution of Eq. (6) is then

$$G_\Omega(\mathbf{r}, \mathbf{r}_0; k_f) = G_\infty(\mathbf{r}, \mathbf{r}_0; k_f) + G_s(\mathbf{r}, \mathbf{r}_s, \mu_b; k_f), \tag{7}$$

where μ_b is the location of the boundary, as depicted in Fig. 3, such that the location of the image source is $\mathbf{r}_s = (\xi_s, \mu_s) = (\xi_0, 2\mu_b - \mu_0)$. The aim of the following is to determine G_s in the most general case, i.e. without assuming any particular set of boundary conditions for the edge.

The integrand of Eq. (5) contains two plane waves travelling from μ_0 in their respective half-planes $\mu > \mu_0$ and $\mu < \mu_0$. The latter represents a plane wave incident on the boundary $\partial\Omega$, located along axis $\mu = \mu_b$, which can be written as

$$w_i(\xi, \mu, \xi_0, \mu_0, \mu_b; k_f) = e^{jk_\xi(\xi - \xi_0)}(Ae^{-j\sqrt{k_f^2 - k_\xi^2}(\mu - \mu_b)} + Be^{\sqrt{k_f^2 + k_\xi^2}(\mu - \mu_b)}), \tag{8}$$

where

$$A = \frac{j}{8\pi k_f^2 D} \frac{e^{-j\sqrt{k_f^2-k_\xi^2}(\mu_b-\mu_0)}}{\sqrt{k_f^2-k_\xi^2}}, \quad B = \frac{j}{8\pi k_f^2 D} \frac{je^{\sqrt{k_f^2+k_\xi^2}(\mu_b-\mu_0)}}{\sqrt{k_f^2+k_\xi^2}}. \tag{9}$$

Similarly, the reflected wave is a superposition of a propagating term and an evanescent term, in the form

$$w_r(\xi,\mu,\xi_0,\mu_0,\mu_b;k_f) = e^{jk_\xi(\xi-\xi_0)}(Ce^{j\sqrt{k_f^2-k_\xi^2}(\mu-\mu_b)} + De^{-\sqrt{k_f^2+k_\xi^2}(\mu-\mu_b)}), \tag{10}$$

where C and D are obtained by applying the boundary conditions to the superposition of incident and reflected waves. The relation between A, B, C and D is then given by

$$\begin{bmatrix} C \\ D \end{bmatrix} = \mathbf{R} \begin{bmatrix} A \\ B \end{bmatrix}, \tag{11}$$

where

$$\mathbf{R}(k_\xi,k_f) = \begin{bmatrix} R_{pp}(k_\xi,k_f) & R_{ep}(k_\xi,k_f) \\ R_{pe}(k_\xi,k_f) & R_{ee}(k_\xi,k_f) \end{bmatrix} \tag{12}$$

is the reflection matrix of the boundary. Each term of the form R_{ir} represents wave conversion from incident wave i to reflected wave r, where i and r denote propagating (p) or evanescent (e) components. The left column of the reflection matrix contains the reflection coefficients for an incident propagating wave and can be obtained by applying the boundary conditions to the superposition of incident and reflected waves w_i and w_r letting $B=0$. The same holds for the right column of the reflection matrix with $A=0$.

The total reflected field G_s is the superposition of an infinite number of elementary waves in the form of Eq. (10) and it is thus obtained by integrating Eq. (10) over $k_\xi \in \mathbb{R}$. A further step consists in interpreting the reflected field as the contribution of the image source to the total flexural wave field. This is done by performing the changes of variables $\xi_s = \xi_0$ and $\mu_b - \mu_0 = -(\mu_b - \mu_s)$ (see Fig. 3). Thus, the image source contribution is obtained in the form

$$G_s(\mathbf{r},\mathbf{r}_s,\mu_b;k_f) = \frac{j}{8\pi k_f^2 D} \int_{-\infty}^{+\infty} e^{jk_\xi(\xi-\xi_s)}$$

$$\begin{bmatrix} e^{j\sqrt{k_f^2-k_\xi^2}(\mu-\mu_b)} & e^{-\sqrt{k_f^2+k_\xi^2}(\mu-\mu_b)} \end{bmatrix} \begin{bmatrix} R_{pp}(k_\xi,k_f) & R_{ep}(k_\xi,k_f) \\ R_{pe}(k_\xi,k_f) & R_{ee}(k_\xi,k_f) \end{bmatrix}$$

$$\begin{bmatrix} \dfrac{e^{j\sqrt{k_f^2-k_\xi^2}(\mu_b-\mu_s)}}{\sqrt{k_f^2-k_\xi^2}} \\[2ex] j\dfrac{e^{-\sqrt{k_f^2+k_\xi^2}(\mu_b-\mu_s)}}{\sqrt{k_f^2+k_\xi^2}} \end{bmatrix} dk_\xi. \tag{13}$$

Eq. (13) represents a sum of plane waves, where the integrand can be interpreted as a wave with a propagating component along axis ξ and both propagating and evanescent components on axis μ, travelling along a distance $\mu_b - \mu_0$, reflected at the boundary $\mu = \mu_b$ and then travelling along a distance $\mu - \mu_b$. The expression of Green's function of the semi-infinite plate G_Ω is then given by Eq. (7), with G_∞ given by Eq. (5) and G_s given by Eq. (13). The applicability of the present approach to a semi-infinite plate with a given set of boundary conditions is subjected to the condition that the corresponding reflection matrix is known in the form appearing in Eq. (13), e.g. as obtained by the methods described in Refs. [22,25,26].

At this point, it should be noted that the present approach for obtaining Green's function of a semi-infinite domain is a generalisation of the classical image source method. In fact, the latter was originally developed given some assumptions on the boundary conditions, which lead to a simplified form of the image source contribution, as detailed hereafter. The first assumption in the classical image source method is that the reflection of a flexural wave on a boundary does not induce conversion between propagating and evanescent components. This renders it applicable only to particular boundary conditions in which the corresponding reflection matrix is diagonal, i.e. the terms R_{ep} and R_{pe} are zero, which simplifies the image source contribution. Another restriction of the classical image source method is the fact that wave reflection on the boundary is assumed to be independent from the angle of incidence of waves or, more generally, from the wavenumber component k_ξ used herein. Thus, considering such assumptions in Eq. (13) yields a simplified form of G_s which is applicable to particular boundary conditions such as the commonly encountered cases of simply supported and roller supported edges, as used in previous studies [19,21]. The explicit expression of the image source contribution in those cases is given in Appendix B.

In the present case, the further generality of the boundary conditions requires the reflected field to be written in the form of Eq. (13). In particular and unlike in the classical image source method, it includes an explicit dependence on the location of the boundary, μ_b, which is necessary in order to account for the coupling between the incident and reflected propagating and evanescent waves.

Table 1
Boundary conditions and corresponding reflection matrices for a simply supported, roller, clamped or free edge at $\mu = \mu_b$.

Boundary conditions		Reflection matrix $\mathbf{R}(k_\xi, k_f)$
Simply supported	$\begin{cases} w(\xi, \mu_b) = 0 \\ M_\mu(\xi, \mu_b) = 0 \end{cases}$	$\begin{bmatrix} -1 & 0 \\ 0 & -1 \end{bmatrix}$
Roller	$\begin{cases} \dfrac{\partial w}{\partial \mu}(\xi, \mu_b) = 0 \\ V_\mu(\xi, \mu_b) = 0 \end{cases}$	$\begin{bmatrix} 1 & 0 \\ 0 & 1 \end{bmatrix}$
Clamped	$\begin{cases} w(\xi, \mu_b) = 0 \\ \dfrac{\partial w}{\partial \mu}(\xi, \mu_b) = 0 \end{cases}$	$\begin{bmatrix} -\dfrac{\sqrt{k_f^2 + k_\xi^2} - j\sqrt{k_f^2 - k_\xi^2}}{\sqrt{k_f^2 + k_\xi^2} + j\sqrt{k_f^2 - k_\xi^2}} & \dfrac{-2\sqrt{k_f^2 + k_\xi^2}}{\sqrt{k_f^2 + k_\xi^2} + j\sqrt{k_f^2 - k_\xi^2}} \\ \dfrac{-2j\sqrt{k_f^2 - k_\xi^2}}{\sqrt{k_f^2 + k_\xi^2} + j\sqrt{k_f^2 - k_\xi^2}} & \dfrac{\sqrt{k_f^2 + k_\xi^2} - j\sqrt{k_f^2 - k_\xi^2}}{\sqrt{k_f^2 + k_\xi^2} + j\sqrt{k_f^2 - k_\xi^2}} \end{bmatrix}$
Free	$\begin{cases} M_\mu(\xi, \mu_b) = 0 \\ V_\mu(\xi, \mu_b) = 0 \end{cases}$	$\begin{bmatrix} \dfrac{ad - bc}{ad + bc} & \dfrac{-2ac}{ad + bc} \\ \dfrac{-2bd}{ad + bc} & -\dfrac{ad - bc}{ad + bc} \end{bmatrix}$ $a = k_f^2 + (1 - v)k_\xi^2$ $b = -k_f^2 + (1 - v)k_\xi^2$ $c = -\sqrt{k_f^2 + k_\xi^2}(k_f^2 - (1 - v)k_\xi^2)$ $d = j\sqrt{k_f^2 - k_\xi^2}(k_f^2 + (1 - v)k_\xi^2)$

3.2. Examples of Green's functions for semi-infinite plates with simply supported, roller supported, clamped or free edges

To the best of our knowledge, the most significant work so far on determining explicit expressions of Green's functions for flexural waves in semi-infinite plates has been done by Gunda et al. [23], where the Green's functions of clamped and free semi-infinite plates are obtained by applying appropriate corrections respectively to the simply supported and roller boundary conditions. Such expressions are thus used as a benchmark for the present approach, as detailed below.

Table 1 summarises the boundary conditions of simply supported, roller, clamped and free edges and their corresponding reflection matrices, where w and $\partial w / \partial \mu$ respectively denote the normal displacement and the slope along direction μ, and

$$M_\mu = -D\left(\frac{\partial^2 w}{\partial \mu^2} + v\frac{\partial^2 w}{\partial \xi^2}\right) \tag{14}$$

and

$$V_\mu = -D\left(\frac{\partial^3 w}{\partial \mu^3} + (2 - v)\frac{\partial^3 w}{\partial \xi^2 \partial \mu}\right) \tag{15}$$

respectively denote the bending moment and the total shear force.

By replacing the reflection matrix of a simply supported, roller, clamped or free edge in Eq. (13), it can be verified that Green's function given by Eq. (7) is identical to Eqs. (19), (22), (44) and (62) of Ref. [23], respectively. The main advantage of the present method is that it provides the Green's function of a semi-infinite plate regardless of the specific boundary conditions, as long as the corresponding reflection matrix is known.

4. Approximation of the Green's function of a convex polygonal plate

4.1. Formulation of the problem

Considering a polygonal plate Ω, as depicted in Fig. 4, the Green's function G_Ω is the solution of the generic set of Eq. (6), where the boundary $\partial \Omega$ forms a closed line and thus yields an infinite number of reflections in the plate, which are in turn described by an infinite number of image sources. In addition to specular wave reflection, described by image sources, the plate corners induce an additional contribution to the field, corresponding to wave diffraction [27,28]. However, the
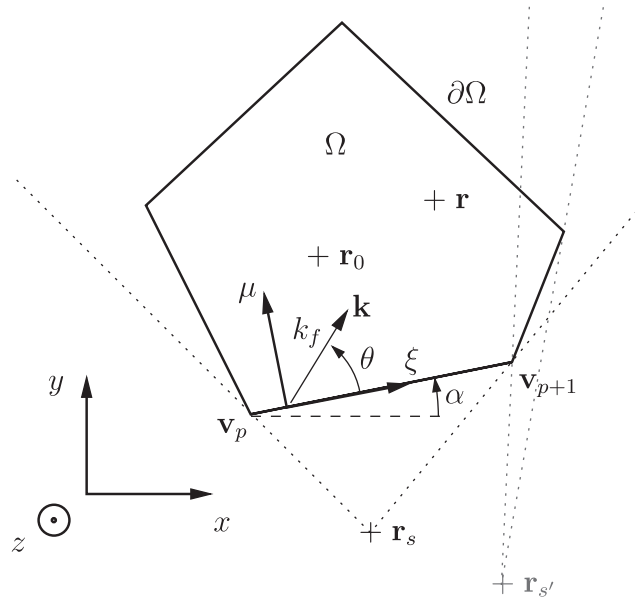
Fig. 4. Green's problem for a convex polygonal plate. $\mathbf{r}_0$, original source; $\mathbf{r}_s$, image source of first order; $\mathbf{r}_{s'}$, image source of second order; $\mathbf{r}$, observation point; $\cdots\cdots$, validity zones of image sources.

corresponding correction terms are significant only at low frequencies, as shown by Gunda et al. [29]. On that account, we propose an approximation of the Green's function of the polygonal plate in the form of a superposition of the contributions from the original source and the image sources, as

$$\tilde{G}_\Omega(\mathbf{r},\mathbf{r}_0;k_f) = G_\infty(\mathbf{r},\mathbf{r}_0;k_f) + \sum_{s=1}^{\infty} G_s(\mathbf{r},\mathbf{r}_s,\mu_b^{(s)};k_f), \tag{16}$$

where the terms G_s represent the contributions of image sources to the displacement field, s being the image source index. The aim of the following is to determine the image source contributions G_s.

4.2. Geometrical construction of image sources

Wave reflections at the boundaries of the domain are described by means of image sources, which are obtained by successive symmetries of the original source on the different plate edges. Thus, for a polygonal plate having N_v vertices, the original source generates N_v sources, one with respect to each edge. Subsequently, each image source generates N_v-1 new image sources. The pattern resulting from such geometrical procedure corresponds to what one would observe by standing with a source of light in a polygonal room made of mirrors. The location of an image source s originating at edge p from a source located at $\mathbf{r}_m$, i.e. its "mother" source, takes the form

$$\mathbf{r}_s = -\mathbf{r}_m + 2\mathbf{v}_p + 2\frac{(\mathbf{r}_m-\mathbf{v}_p)\cdot(\mathbf{v}_{p+1}-\mathbf{v}_p)}{\left|\mathbf{v}_{p+1}-\mathbf{v}_p\right|^2}(\mathbf{v}_{p+1}-\mathbf{v}_p), \tag{17}$$

where $\mathbf{v}_p$ and $\mathbf{v}_{p+1}$ are the locations of the vertices of the generator edge, as illustrated in Fig. 4.

Furthermore, the edges of the plate are of finite length. As shown by Mechel [20], the reflected field giving rise to a given image source is therefore valid in the zone delimited by the image source position $\mathbf{r}_s$ and the vertices $\mathbf{v}_p$ and $\mathbf{v}_{p+1}$ of the generator edge, as represented by the dotted lines in Fig. 4. The geometrical validity conditions of an image source located at $\mathbf{r}_s$ for an observation point $\mathbf{r}$ are given by

$$\begin{cases} ((\mathbf{v}_{p+1}-\mathbf{r}_s)\times(\mathbf{r}-\mathbf{r}_s))\cdot\mathbf{z} > 0, & \text{(a)} \\ ((\mathbf{r}-\mathbf{r}_s)\times(\mathbf{v}_p-\mathbf{r}_s))\cdot\mathbf{z} > 0, & \text{(b)} \end{cases} \tag{18}$$

where $\times$ denotes cross product and $\mathbf{z}$ is the unitary vector such that $(\mathbf{x},\mathbf{y},\mathbf{z})$ forms a right-handed basis. The validity conditions are included in a function $V(\mathbf{r},\mathbf{r}_s)$ such that

$$V(\mathbf{r},\mathbf{r}_s) = \begin{cases} 1 & \text{in the validity zone,} \\ 0 & \text{elsewhere}. \end{cases} \tag{19}$$

4.3. First wave reflection on the boundaries

The contributions of the image sources of first order, i.e. directly generated from the original source at each one of the edges, can be computed using the approach developed above for semi-infinite plates, i.e. from Eq. (13), using a local coordinate system (ξ,μ) for each edge. Each image source contribution is then valid in the area defined by function $V(\mathbf{r},\mathbf{r}_s)$. For a plate having N_ν vertices, the contributions of image sources of first order, i.e. the first N_ν image sources, can be expressed as

$$G_s^{(\mathrm{I})}(\mathbf{r},\mathbf{r}_s,\mu_b^{(s)};k_f) = V(\mathbf{r},\mathbf{r}_s)\frac{j}{8\pi k_f^2 D}\int_{-\infty}^{+\infty} e^{jk_\xi(\xi-\xi_s)}[e^{j\sqrt{k_f^2-k_\xi^2}(\mu-\mu_b^{(s)})}\quad e^{-\sqrt{k_f^2+k_\xi^2}(\mu-\mu_b^{(s)})}]$$

$$\begin{bmatrix} R_{pp}^{(s)}(k_\xi,k_f) & R_{ep}^{(s)}(k_\xi,k_f) \\ R_{pe}^{(s)}(k_\xi,k_f) & R_{ee}^{(s)}(k_\xi,k_f) \end{bmatrix}\begin{bmatrix} \dfrac{e^{j\sqrt{k_f^2-k_\xi^2}(\mu_b^{(s)}-\mu_s)}}{\sqrt{k_f^2-k_\xi^2}} \\ j\dfrac{e^{-\sqrt{k_f^2+k_\xi^2}(\mu_b^{(s)}-\mu_s)}}{\sqrt{k_f^2+k_\xi^2}} \end{bmatrix} dk_\xi, \tag{20}$$

where $\mu = \mu_b^{(s)}$ defines the boundary giving rise to source s in the local coordinate system (ξ,μ), i.e. the symmetry axis between $\mathbf{r}_0$ and $\mathbf{r}_s$, and $R_{ir}^{(s)}$ are the different terms of the corresponding reflection matrix, which couples incident (i) waves from the original source to reflected (r) waves.

4.4. Second and subsequent wave reflections on the boundaries

The contribution of an image source of first order acts in turn as the incident field on another boundary and generates an image source of second order. The exact form of the contribution of an image source of second order cannot be derived using the same procedure as for image sources of first order and an approximation is proposed, as detailed in the following. In the above derivation, leading to the contribution of an image source of first order, the incident and reflected fields are considered as sums of plane waves expressed in the local coordinate system (ξ,μ) of the edge where the reflection occurs. The incident and reflected plane waves are written in a separated-variable form in Eqs. (8) and (10), respectively, which both include a propagating component along the ξ axis and a superposition of propagating and evanescent components along the μ axis, making it possible to use a reflection matrix for plane waves, Eq. (12). However, a propagating wave with amplitude decreasing along its front cannot be written in such separated-variable form using two different coordinate systems in the general case, as detailed in Appendix C. As a consequence, an individual plane wave resulting from the first reflection, i.e. Eq. (10), cannot be written in the form of Eq. (8) in the local coordinate system of another edge where a second reflection may take place. Therefore, the contribution of image sources of second and higher orders cannot be obtained in its complete form from the concept of individual plane wave reflection. For the purposes of the present paper, no attempt is made to compute the exact expression, which would require a rather different approach. However, the wavelength being sufficiently short compared to the plate dimensions, the evanescent components can be neglected, thus solving the difficulty of the coordinate change. The contributions of the image sources associated to the second and subsequent wave reflections on the boundaries are then approximated by their propagating component, in the form

$$G_s^{(\mathrm{II})}(\mathbf{r},\mathbf{r}_s;k_f) = V(\mathbf{r},\mathbf{r}_s)\frac{j}{8\pi k_f^2 D}\int_{-|k_f|}^{|k_f|} e^{jk_\xi(\xi-\xi_s)}A_{pp}^{(s)}(k_\xi,k_f)\frac{e^{j\sqrt{k_f^2-k_\xi^2}(\mu-\mu_s)}}{\sqrt{k_f^2-k_\xi^2}} dk_\xi, \tag{21}$$

where $A_{pp}^{(s)}$ is the amplitude weight of image source s, resulting from the successive reflections of propagating waves. In the considered integration domain, defined by $-|k_f| < k_\xi < |k_f|$, the transverse wavenumber coordinate $k_\mu = \sqrt{k_f^2-k_\xi^2}$ is real, as shown in Fig. 2, such that the wavenumber coordinates k_ξ and k_μ are related to the flexural wavenumber by

$$k_f^2 = k_\xi^2 + k_\mu^2. \tag{22}$$

Alternatively, the use of wavenumber polar coordinates yields

$$k_\xi = |k_f|\cos(\theta), \tag{23}$$

where θ is the orientation of the plane propagating wave defined by k_ξ with respect to the reflecting edge, as shown in Fig. 4. Thus, the amplitude weight $A_{pp}^{(s)}$ is obtained as the product of the scalar reflection coefficients R_{pp} of the edges that successively participate in the construction of image source s, in the form

$$A_{pp}^{(s)}(\theta) = \prod_{n=1}^{N(s)} R_n^{(s)}(\theta,\alpha_n), \tag{24}$$

where $n = 1, \ldots, N(s)$ denotes the order of reflection on edges for each image source s and α_n is the orientation of edge n with respect to the global coordinate system (x,y), as illustrated in Fig. 4.

At this point it is important to notice that some particular types of edges present reflection properties that are independent from the angle of incidence of waves and do not induce wave conversion, which implies that the associated reflection matrix is constant and diagonal. This is the case for simply supported and roller supported edges, for example. For plates having exclusively such kinds of boundary conditions, each image source contribution is obtained simply from the product of the contribution of its mother source by the reflection coefficient of the edge, as detailed in Appendix B. In those cases, the exact form of the contribution of an image source of any reflection order is known and there is no need of neglecting evanescent waves.

4.5. Approximated Green's function and domain of applicability

The approximated Green's function of the polygonal plate is obtained from Eq. (16), by considering Eqs. (5), (20) and (21) for the original source, first and second-order image sources, respectively, in the form

$$\tilde{G}_\Omega(\mathbf{r},\mathbf{r}_0;k_f) = G_\infty(\mathbf{r},\mathbf{r}_0;k_f) + \sum_{s=1}^{N_v} G_s^{(I)}(\mathbf{r},\mathbf{r}_s,\mu_b^{(s)};k_f) + \sum_{s=N_v+1}^{\infty} G_s^{(II)}(\mathbf{r},\mathbf{r}_s;k_f), \tag{25}$$

where N_v is the number of vertices or edges of the plate. The solution is then known for arbitrary boundary conditions as long as the reflection matrix of the edges are known in the form of Eq. (12). The obtained Green's function is an approximation based on neglecting evanescent waves in the calculation of the contributions of second-order image sources, $G_s^{(II)}$. In fact, the displacement field related to the terms $R_{ep}(k_\xi,k_f)$, $R_{pe}(k_\xi,k_f)$ and $R_{ee}(k_\xi,k_f)$ of the reflection matrices is of low amplitude as long as both the source and the observation point are sufficiently distant from the edges. As a consequence, the proposed solution is inaccurate in the nearfield of the edges. In particular, the approach is not adapted to plates including sharp angles, since a given edge may be in the nearfield of another edge, leading to cumulative errors in the construction of image sources. The convergence of the series in Eq. (25) is then subjected to the distance from the source (and/or the observation point) to the edges, relatively to the wavelength. Furthermore, the damping ratio η of the plate material also governs the convergence of the solution since a low number of reflections is needed to accurately compute the field in a highly damped plate.

5. Numerical implementation

In this section, the numerical implementation of Eq. (25) is discussed. By formulating Eq. (21) as

$$G_s^{(II)}(\mathbf{r},\mathbf{r}_s;k_f) = V(\mathbf{r},\mathbf{r}_s)\frac{j}{8\pi k_f^2 D}\int_{-\infty}^{\infty} u\left(\frac{k_\xi}{2|k_f|}\right) e^{jk_\xi(\xi-\xi_s)} A_{pp}^{(s)}(k_\xi,k_f)\frac{e^{j\sqrt{k_f^2-k_\xi^2}(\mu-\mu_s)}}{\sqrt{k_f^2-k_\xi^2}} \, dk_\xi, \tag{26}$$

where

$$u\left(\frac{k_\xi}{2|k_f|}\right) = \begin{cases} 1, & k_\xi \in [-|k_f|,|k_f|], \\ 0 & \text{elsewhere} \end{cases} \tag{27}$$

is the rectangular window function of span $2|k_f|$ centred on $k_\xi = 0$, the integral in Eqs. (20) and (26) is interpreted as an one-dimensional inverse spatial Fourier transform from wavenumber coordinate k_ξ to space coordinate ξ. The numerical
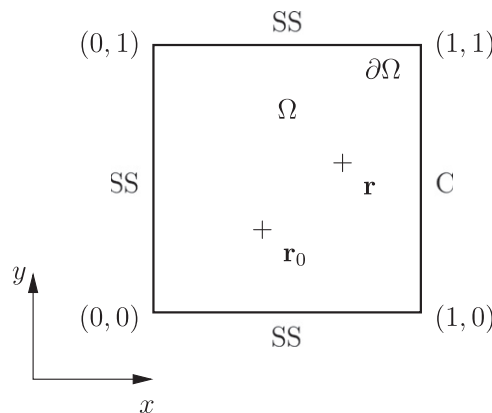
Fig. 5. Square plate with three simply supported (SS) edges and one clamped (C) edge.

implementation of such expressions is performed by using discrete inverse spatial Fourier transform in order to take advantage of a fast Fourier transform algorithm in terms of computational efficiency.

Furthermore, practical implementation requires the image source series to be truncated. Thus, image sources outside a truncation circle of radius r_t are ignored. The dimensionless parameter γ is used for controlling the truncation distance with respect to an arbitrary characteristic length r_c of the plate, in the form

$$\gamma = \frac{r_t}{r_c}, \tag{28}$$
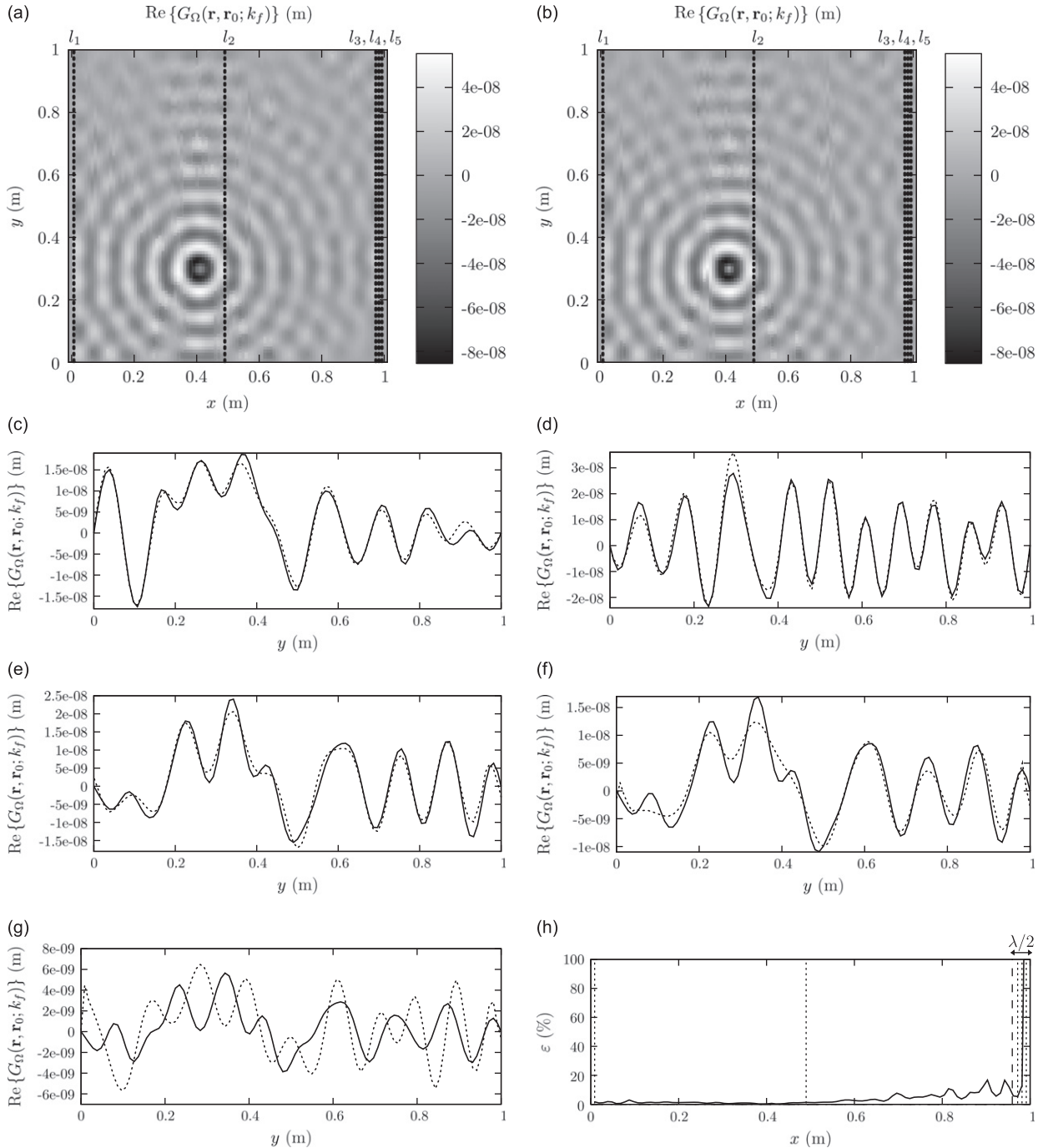
Fig. 6. Amplitude of Green's function for the square plate. (a) Exact; (b) proposed method; (c)–(g) displacement field on vertical lines l_1 to l_5; —, exact; ·····, proposed method. (h) Error as a function of abscissa, from Eq. (30).

where, by respectively denoting S and p the total area and the perimeter of the plate, r_c is taken as

$$r_c = \frac{\pi S}{p}, \tag{29}$$

which is the average distance between two successive image sources, also referred to as the mean free path of waves in the plate [12].

6. Results

In this section, the harmonic responses of different polygonal plates with various boundary conditions are computed and compared to exact or numerical solutions of reference. The main purpose is to validate the present method and to evaluate the errors due to neglecting edge effects. Two plates are tested: a Levy-type plate, for which the analytical Green's function is known, and an arbitrary polygonal plate, for which the response is computed by using the finite element method (FEM). For both plates, one edge is clamped and the others are simply supported.

6.1. Levy-type plate: comparison to the exact solution

There exist only few sets of boundary conditions leading to an analytical expression of the response of a polygonal plate [6]. Rectangular plates with two opposite edges simply supported, i.e. Levy-type plates, are well-known configurations allowing an analytical solution [7,22]. A square plate, as shown in Fig. 5, is here considered, with simply supported edges along $y=0$, $y=L$ and $x=0$, and a clamped edge along $x=L$.

In the following, the side length of the plate is $L=1$ m and the thickness is $h=2$ mm. The plate material is steel, with density $\rho = 7850$ kg m^{-3}, Young's modulus $E_0 = 210$ GPa and Poisson's ratio $\nu = 0.3$. The structural damping ratio is chosen as $\eta = 0.07$. The plate is excited by a harmonic point source at $\mathbf{r}_0 = (0.41$ m$,0.3$ m$)$ at the frequency $f = 3$ kHz. At this frequency, the modal overlap factor [21] is equal to 42, i.e. there is an average of 42 resonances in a -3 dB resonance band, which indicates that the computation is done in a significantly high-frequency regime. The solution of reference is obtained analytically by classical modal superposition [22], to which is compared the solution obtained by the proposed method, with $\gamma = 6$ (488 sources). The number of points for the fast Fourier transform is $N_F=1024$.

In order to quantify the accuracy of the proposed method, an error indicator is computed for each vertical line of the plate, as

$$\varepsilon(x) = \frac{\sum_{i=1}^{N} \left| w(x,y_i) - w^{(\mathrm{ref})}(x,y_i) \right|^2}{\sum_{i=1}^{N} \left| w^{(\mathrm{ref})}(x,y_i) \right|^2}, \tag{30}$$

where N is the number of points on the vertical line at abscissa x and where $w(x,y_i)$ and $w^{(\mathrm{ref})}(x,y_i)$ are respectively the displacement fields obtained by the present method and from the reference solution. Eq. (30) thus represents a mean quadratic error on each vertical line of the plate, normalised by the mean quadratic value of the reference solution.

Fig. 6(a) and (b) shows the real part of the Green's function, respectively obtained by the exact solution and the proposed approximation. Fig. 6(c)–(g) shows the displacement field on vertical lines l_1 to l_5, respectively defined by $x_1 = 0.013L$, $x_2 = 0.484L$, $x_3 = 0.956L$, $x_4 = 0.972L$ and $x_5 = 0.987L$. Furthermore, Fig. 6(h) shows the error ε as a function of x. The agreement is satisfactory in the whole plate, except near the clamped edge, within a distance comparable to half the wavelength, which in the present case is equal to $\lambda/2 = 0.0405L = 4.05$ cm.
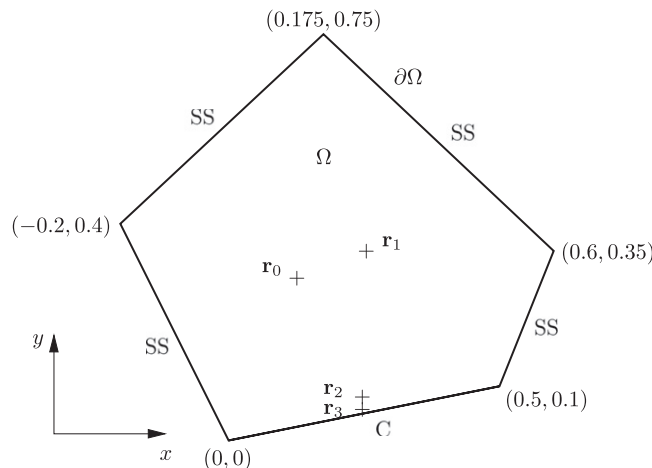
Fig. 7. Polygonal plate for comparison of the proposed approach to FEM with clamped (C) and simply supported (SS) boundaries. $\mathbf{r}_0 = (0.125,0.3)$, source; $\mathbf{r}_1 = (0.245778,0.350778)$, $\mathbf{r}_2 = (0.245778,0.073775)$ and $\mathbf{r}_3 = (0.245778,0.058386)$, observation points. Coordinates are in meters.

Simply supported edges do not induce wave conversion between propagating and evanescent components, as observed in the corresponding reflection matrix in Table 1. In fact, edge effects near such boundaries are of low influence on the global displacement field since they correspond to pure evanescent waves generated at the source that reflect back. On the other hand, as recalled in Table 1, the reflection matrix of the clamped edge involves wave conversion between propagating and evanescent waves. Thus, propagating waves incident on the clamped boundary give rise to evanescent waves, which are neglected for sources of second and higher orders. As a consequence, higher discrepancies appear near the clamped edge.

6.2. Arbitrary polygonal plates: comparison to FEM

In order to validate the proposed method in a more general configuration, an arbitrary polygonal plate is considered, as shown in Fig. 7.

The response of the plate is computed as a function of frequency at three different observation points, $\mathbf{r}_1$, $\mathbf{r}_2$ and $\mathbf{r}_3$, for a point source at $\mathbf{r}_0$, for two different values of the structural damping ratio, $\eta = 0.07$ and $\eta = 0.14$, by the proposed method and by FEM.
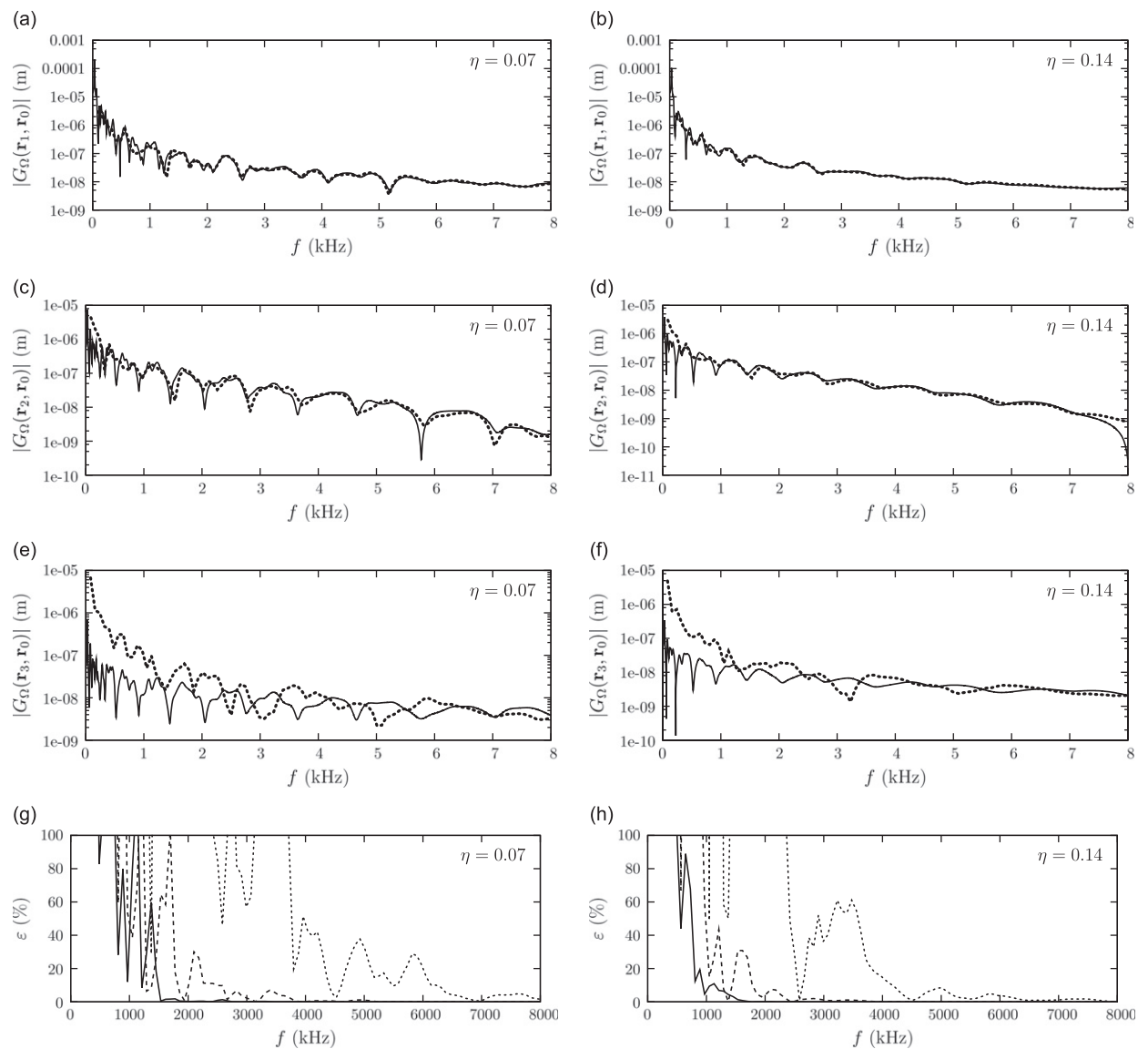
Fig. 8. Modulus of Green's function of the polygonal plate as a function of frequency computed by the proposed method ($\cdots\cdots$) and by FEM (—), for $\eta = 0.07$ (left column) and $\eta = 0.14$ (right column), at points (a,b) $\mathbf{r}_1$, (c,d) $\mathbf{r}_2$ and (e,f) $\mathbf{r}_3$. (h,g) Error at points: —, $\mathbf{r}_1$; - - - - -, $\mathbf{r}_2$; $\cdots\cdots$, $\mathbf{r}_3$.

For obtaining the plate response as a function of frequency, the computation detailed above is performed at 99 different frequencies, from 80 Hz to 8 kHz, with the truncation parameter set to $\gamma = 4$. The number of points of the fast Fourier transform is $N_F = 1024$. A total of 46 056 nodes is considered in the finite element model, giving rise to 91 319 linear triangular elements. The average element length is 3 mm and the eigenmodes are computed up to the frequency 12 kHz, at which the wavelength is greater than 13 times the average element length.

The error of the response for a given observation point in the plate is computed by using an indicator as a function of frequency, given by

$$\varepsilon(f) = \frac{|w(f) - w^{(\mathrm{ref})}(f)|^2}{\frac{1}{N}\sum_{i=1}^{N} |w^{(\mathrm{ref})}(f_i)|^2}, \tag{31}$$

where N is the number of frequencies for the computation of the response and $w(f)$ and $w^{(\mathrm{ref})}(f)$ are the responses computed, respectively, by the proposed method and by FEM at a given point. Eq. (31) thus represents the quadratic error at each frequency, normalised by the mean quadratic value of the reference solution over the frequency range of the simulations.

Fig. 8 shows the modulus of Green's function as a function of frequency, for the chosen parameters. The computed responses are in accordance with the finite element predictions in the central region of the plate, as observed on the displacement fields at the selected observation points $\mathbf{r}_1$ and $\mathbf{r}_2$. As the observation point reaches the clamped boundary at point $\mathbf{r}_3$, the image source method no longer predicts the field accurately. Moreover, Fig. 8 shows that the accuracy of the proposed method increases with frequency and structural damping ratio. That is to say that, for a given accuracy to be reached, the number of needed image sources decreases with frequency and damping. Such behaviour of the accuracy is opposite to that of the finite element method, which is limited in terms of computational time to low frequencies and high quality factors.

7. Conclusion

This paper provides a method for obtaining the harmonic Green's function of the flexural vibrations of thin semi-infinite plates and an approximation of Green's function of convex polygonal plates by using a generalised image source method. The latter consists in considering the Green's function of a semi-infinite or finite domain as the superposition of the contributions from the original source and its image sources with respect to the boundaries, which represent successive wave reflections. The original source contribution is described by the infinite plate Green's function, and is written as a continuous sum of propagating and evanescent plane waves, incident on the boundaries. The contributions of image sources thus arise as continuous sums of reflected plane waves. For semi-infinite plates, a general expression of the exact Green's function is obtained for arbitrary boundary conditions, as long as the reflection matrix of the boundary is known. For polygonal plates, the image sources representing the first reflection at each one of the edges are obtained from the Green's function of the corresponding semi-infinite plate in the local coordinate system of the edge at which reflection occurs. The plane waves therein are in a separated variable form that cannot be transposed to local coordinate systems of other edges. Therefore, the contributions of image sources representing the second and subsequent reflections on boundaries cannot be obtained in their complete form. However, after the second reflection and at high frequencies, the distance travelled by waves is much larger than their wavelength. An approximation of the Green's function is then written by neglecting evanescent waves in the calculation of the image sources of second and subsequent orders. Comparisons to exact and finite element method simulated responses show that the displacement field is accurately predicted outside the nearfield area of the edges, which decreases with frequency and structural damping. The approximations of the Green's functions obtained by the proposed method are applicable to any set of boundary conditions of which the reflection matrices are known.

A significant advantage of the method developed in this paper is that wave propagation, geometry and boundary conditions can be treated separately. Work is ongoing along this direction for using it as a tool for modelling and characterising mid- and high-frequency vibrations of plates of complex shapes and arbitrary boundary conditions.

Appendix A. Green's function of an infinite plate in rectangular coordinates

By defining one-dimensional spatial Fourier transform and inverse transform as

$$\overline{w}(k_\xi, \mu) = \mathcal{F}_\xi[w(\xi, \mu)] = \frac{1}{\sqrt{2\pi}} \int_{-\infty}^{+\infty} w(\xi, \mu) \mathrm{e}^{-jk_\xi \xi} \, \mathrm{d}\xi \tag{32}$$

and

$$w(\xi, \mu) = \mathcal{F}_\xi^{-1}[\overline{w}(k_\xi, \mu)] = \frac{1}{\sqrt{2\pi}} \int_{-\infty}^{+\infty} \overline{w}(k_\xi, \mu) \mathrm{e}^{jk_\xi \xi} \, \mathrm{d}k_\xi. \tag{33}$$

Fourier transform of Eq. (1) yields

$$D\left(\frac{\partial^4}{\partial\mu^4}-2k_\xi^2\frac{\partial^2}{\partial\mu^2}+k_\xi^4-k_f^4\right)\overline{G}_\infty(k_\xi,\mu,\xi_0,\mu_0;k_f)=\frac{\mathrm{e}^{-jk_\xi\xi_0}}{\sqrt{2\pi}}\delta(\mu-\mu_0).\tag{34}$$

Using the associated homogeneous equation and taking into account Sommerfeld radiation condition [24] and the continuity of the displacement field at $\mu=\mu_0$ yields the Fourier transform of Green's function in the form

$$\overline{G}_\infty(k_\xi,\mu,\xi_0,\mu_0;k_f)=A\mathrm{e}^{jk_\mu^{(1)}|\mu-\mu_0|}+B\mathrm{e}^{jk_\mu^{(2)}|\mu-\mu_0|},\tag{35}$$

where

$$k_\mu^{(1)}=\sqrt{k_f^2-k_\xi^2},\quad k_\mu^{(2)}=j\sqrt{k_f^2+k_\xi^2}.\tag{36}$$

The expressions of A and B are obtained by integrating Eq. (34) on the interval $\mu\in[\mu_0-\varepsilon,\mu_0+\varepsilon]$ with $\varepsilon\rightarrow0$ and using the property of continuity of the slope at μ_0. Green's function in the spatial domain is then obtained by inverse Fourier transform and is given in Eq. (5).

Appendix B. Image source contribution in the case of reflection without angular dependence

The purpose of this appendix is to give the expression of the image source contribution used in the classical image source method, which arises as a particular case of the approach proposed herein, in the case where the boundary conditions are described by a reflection matrix of the form

$$\mathbf{R}(k_\xi,k_f)=\begin{bmatrix}R&0\\0&R\end{bmatrix}.\tag{37}$$

This is the case in particular for simply supported ($R=-1$) or roller ($R=1$) boundary conditions (see Table 1).

For a semi-infinite plate, it can be observed from Eq. (13) that, in the particular case of a reflection matrix proportional to the identity matrix, the image source contribution is described by the infinite plate Green's function multiplied by the constant reflection coefficient, as

$$G_s(\mathbf{r},\mathbf{r}_s;k_f)=RG_\infty(\mathbf{r},\mathbf{r}_s;k_f),\quad\mathbf{r}\in\Omega.\tag{38}$$

It is worth noting that the position of the boundary only appears implicitly in the location of the image source in Eq. (38) due to the absence of coupling between propagating and evanescent components.

In the case of a polygonal plate in which the reflection matrices of the different boundaries are in the form of Eq. (37), the integrand of Eq. (20) can be written in the form of Eq. (8) in the local coordinate system of the edge at which a second reflection may take place. Thus, the contributions from image sources of any reflection order can be written as

$$G_s(\mathbf{r},\mathbf{r}_s;k_f)=V(\mathbf{r},\mathbf{r}_s)A^{(s)}G_\infty(\mathbf{r},\mathbf{r}_s;k_f),\quad\mathbf{r}\in\Omega,\tag{39}$$

where $A^{(s)}$ is the amplitude weight of source s and is independent from the wavenumber coordinate k_ξ. The amplitude weight of source s is given by

$$A^{(s)}=\prod_{n=1}^{N(s)}R_n^{(s)},\tag{40}$$

in which $R_n^{(s)}$ is the reflection coefficient of the edge number n that is needed for the construction of source s. Furthermore, boundaries characterised by a reflection matrix satisfying Eq. (37) are a particular case allowing the calculation of exact Green's functions of several polygonal geometries, as shown in a previous paper [21].

Appendix C. Impossibility of variable separation for waves of multiple types in two different coordinate systems

As mentioned in Section 4.4, a wave that is propagating in one direction of space and attenuating in another cannot be written in a separated-variable form in two different coordinate systems in the general case. This appendix aims at
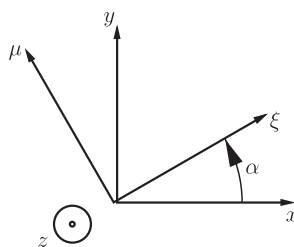
Fig. 9. Two coordinate systems with different orientations.

showing that explicitly. Two coordinate systems differing from an angle α by rotation about the z axis are considered, as shown in Fig. 9.

A plane wave can be represented in coordinate system (ξ,μ) by the separated-variable expression

$$w(\xi,\mu) = e^{jk_\xi \xi} e^{jk_\mu \mu}, \quad k_\xi \in \mathbb{R}, \quad k_\mu \in \mathbb{C}, \tag{41}$$

where $k_\mu = k_\mu^{(1)} = \sqrt{k_f^2 - k_\xi^2}$ or $k_\mu = k_\mu^{(2)} = j\sqrt{k_f^2 + k_\xi^2}$. The coordinate change

$$\begin{cases} \xi = x \cos(\alpha) + y \sin(\alpha), \\ \mu = -x \sin(\alpha) + y \cos(\alpha) \end{cases} \tag{42}$$

yields the expression of w in coordinate system (x,y) as

$$w(x,y) = e^{(jk_\xi \cos(\alpha) - jk_\mu \sin(\alpha))x} e^{(jk_\xi \sin(\alpha) + jk_\mu \cos(\alpha))y}. \tag{43}$$

It is easily observed that there does not exist a pair (k_x,k_y) that satisfies

$$e^{jk_x x} e^{jk_y y} = e^{jk_\xi \xi} e^{jk_\mu \mu}, \quad k_x \in \mathbb{R}, \quad k_y \in \mathbb{C}. \tag{44}$$

References

[1] L.A. Bergman, J.K. Hall, G.G.G. Lueschen, D.M. McFarland, Dynamic Green's functions for Levy plates, *Journal of Sound and Vibration* 162 (2) (1993) 281–310.
[2] R.D. Blevins, *Formulas for Natural Frequencies and Mode Shape*, Krieger, 1993.
[3] D.J. Gorman, *Vibration Analysis of Plates by the Superposition Method*, World Scientific, Singapore, 1999.
[4] S.W. Kang, Free vibration analysis of arbitrarily shaped plates with a mixed boundary condition using non-dimensional dynamic influence functions, *Journal of Sound and Vibration* 256 (3) (2002) 533–549.
[5] S.W. Kang, S.N. Atluri, Free vibration analysis of arbitrarily shaped polygonal plates with simply supported edges using a sub-domain method, *Journal of Sound and Vibration* 327 (3–5) (2009) 271–284.
[6] A. Leissa, *Vibration of Plates*, NASA, Washington, DC, 1969.
[7] W. Soedel, *Vibrations of Shells and Plates*, Marcel Dekker, New York, 2004.
[8] L. Lyamshev, The theory of vibrations of nonhomogeneous elastic plates, *Soviet Physics—Acoustics* 10 (1) (1964) 65–69.
[9] M. Stern, A general boundary integral formulation for the numerical solution of plate bending problems, *International Journal of Solids and Structures* 15 (1979) 769–782.
[10] F. Hartmann, R. Zotemantel, The direct boundary element method in plate bending, *International Journal for Numerical Methods in Engineering* 23 (1986) 2049–2069.
[11] O. Zienkiewicz, R. Taylor, *The Finite Element Method for Solid and Structural Mechanics*, Butterworth-Heinemann, 2005.
[12] R.H. Lyon, R.G. Dejong, *Theory and Application of Statistical Energy Analysis*, Butterworth-Heinemann, Boston, 1995.
[13] A.L. Bot, V. Cotoni, Validity diagrams of statistical energy analysis, *Journal of Sound and Vibration* 329 (2) (2010) 221–235.
[14] F.J. Fahy, Statistical energy analysis: a critical overview, *Philosophical Transactions: Physical Sciences and Engineering* 346 (1681) (1994) 431–447.
[15] K.-S. Chae, J.-G. Ih, Prediction of vibrational energy distribution in the thin plate at high-frequency bands by using the ray tracing method, *Journal of Sound and Vibration* 240 (2) (2001) 263–292.
[16] B. Mace, D. Duhamel, M. Brennan, L. Hinke, Finite element prediction of wave motion in structural waveguides, *Journal of the Acoustical Society of America* 117 (5) (2005) 2835–2843.
[17] C. Vanmaele, D. Vandepitte, W. Desmet, An efficient wave based prediction technique for plate bending vibrations, *Computer Methods in Applied Mechanics and Engineering* 196 (33–34) (2007) 3178–3189.
[18] A.L. Bot, A. Bocquillet, Comparison of an integral equation on energy and the ray-tracing technique in room acoustics, *The Journal of the Acoustical Society of America* 108 (4) (2000) 1732–1740, doi:10.1121/1.1287848.
[19] R. Gunda, S.M. Vijayakar, R. Singh, Method of the images for the harmonic response of beams an rectangular plates, *Journal of Sound and Vibration* 185 (2) (1995) 791–808.
[20] F.P. Mechel, Improved mirror source method in room acoustics, *Journal of Sound and Vibration* 256 (6) (2002) 873–940.
[21] J. Cuenca, F. Gautier, L. Simon, The image source method for calculating the vibrations of simply supported convex polygonal plates, *Journal of Sound and Vibration* 322 (4–5) (2009) 1048–1069.
[22] K.J. Graff, *Wave Motion in Elastic Solids*, Dover, New York, 1991.
[23] R. Gunda, S.M. Vijayakar, R. Singh, J.E. Farstad, Harmonic Green's functions of a semi-infinite plate with clamped or free edges, *Journal of the Acoustical Society of America* 103 (2) (1998) 888–899.
[24] A. Sommerfeld, *Partial Differential Equations in Physics: Lectures on Theoretical Physics*, Academic Press, New York, 1949.
[25] B. Mace, Wave reflection and transmission in beams, *Journal of Sound and Vibration* 97 (2) (1984) 237–246.
[26] Z. Wang, A. Norris, Waves in cylindrical shells with circumferential submembers: a matrix approach, *Journal of the Acoustical Society of America* 181 (3) (1995) 457–484.
[27] V.A. Borovikov, Flexural plane wave scattering by the thin elastic quarter plane in the case of pinched boundary, in: *Days on Diffraction 2006*, IEEE, St. Petersburg2006, pp. 49–63.
[28] V.A. Borovikov, The scattering of a plane flexural wave by a sector of a thin elastic plate with a supported edge, *Journal of Applied Mathematics and Mechanics* 71 (3) (2007) 449–452.
[29] R. Gunda, S.M. Vijayakar, R. Singh, Flexural vibration of an infinite wedge, *Journal of the Acoustical Society of America* 102 (1) (1997) 326–334.